Multi-dimensional deconvolution applied to ambient-noise seismic interferometry

Joost van der Neut[1], Elmer Ruigrok[1], Deyan Draganov[1] and Kees Wapenaar[1],*
[1]Delft University of Technology, Department of Geotechnology.

Summary
A major assumption for retrieving the earth's reflection response with seismic interferometry by cross-correlation of ambient noise is that subsurface sources are uniformly distributed. It has been shown that interferometry by multi-dimensional deconvolution can cope with non-uniform source arrays, but implementation of this concept requires a separation of the incident wavefield from the free-surface multiples. For transient passive sources, this separation can be implemented by time-gating in the recorded transmission panels before cross-correlation, but such methodology cannot be applied for simultaneously acting noise sources. Here we show that time-gating can also be applied after an intermediate cross-correlation step. In cross-correlated data, we isolate events around t=0, which inhabit the illumination imprint of the subsurface sources, the so-called point spread function. Next, we apply multi-dimensional deconvolution with the isolated events to the events away from t=0. In this way we can effectively correct for the effects of a non-uniform subsurface source distribution in data that is already cross-correlated. With this new approach, multi-dimensional deconvolution becomes feasible for simultaneously acting noise sources.

Introduction
With passive seismic interferometry we can retrieve the earth's reflection response by crosscorrelation of ambient-noise recordings (Draganov et al., 2009). One of the major assumptions underpinning this concept is that the noise sources are uniformly distributed throughout the subsurface, which is often not the case in practice. To overcome this problem, Wapenaar et al. (2008) suggested replacing cross-correlation by multi-dimensional deconvolution. The implementation of their idea requires separation of the passive incident wavefields from their free-surface-related multiples through time-gating. For this reason, applications have been limited to transient sources with a distinct incident arrival. An alternative is to introduce the incident wavefields of the passive sources as additional unknowns in the inversion process, as suggested by van Groenestijn and Verschuur (2009). Here we take a different, but practical, approach by showing that time-gating can be implemented after cross-correlation but before inversion. This idea opens the way for applying multi-dimensional deconvolution to simultaneously acting noise sources.

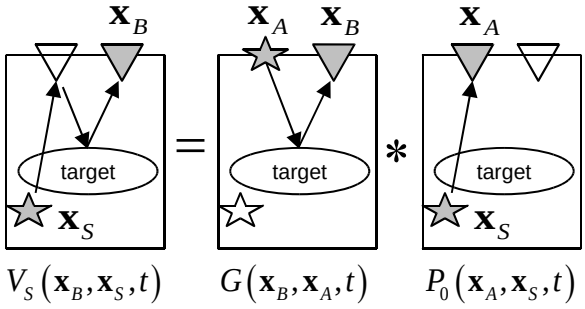

Figure 1: Illustration of the forward model for passive seismic interferometry by multi-dimensional deconvolution; $\mathbf{x}_S$ denotes a subsurface source location, whereas $\mathbf{x}_A$ and $\mathbf{x}_B$ are receivers.

The underlying forward model is shown in Figure 1. The incidence pressure field $\hat{P}_0$ at receiver $\mathbf{x}_A$ is convolved (in the frequency domain, denoted by a hat and frequency ω, this is multiplication) with the unknown Green's function $\hat{G}$ (between virtual source $\mathbf{x}_A$ and receiver $\mathbf{x}_B$) to produce the scattered particle velocity field $\hat{V}_S$ in $\mathbf{x}_B$ (Wapenaar et al., 2008):

$$\hat{V}_S(\mathbf{x}_B,\mathbf{x}_S,\omega) = \int_{\partial D_{rec}} \hat{G}(\mathbf{x}_B,\mathbf{x}_A,\omega)\hat{P}_0(\mathbf{x}_A,\mathbf{x}_S,\omega)\,d^2\mathbf{x}_A. \quad (1)$$

where $\mathbf{x}_S$ is the source location and the integral is over the virtual-source coordinates $\mathbf{x}_A$. Seismic interferometry by multi-dimensional deconvolution is accomplished by inverting equation 1 for $\hat{G}$, given $\hat{P}_0$ and $\hat{V}_S$. $\hat{P}_0$ can be estimated from the time-gated incident particle velocity field $\hat{V}_0$ through $\hat{P}_0 = (\rho c/\cos\phi)\hat{V}_0$, where ρ is the density, *c* the wave velocity and ϕ the propagation angle with respect to normal to the surface. To achieve independence from subsurface source information, we assume that $\cos\phi \approx 1$(wave propagation near-normal incidence) such that $\hat{P}_0 \approx \rho c\hat{V}_0$. Least-squares inversion of equation 1 under substitution of $\hat{P}_0 \approx \rho c\hat{V}_0$ is equivalent to solving the following normal equation (Menke, 1989):

$$\sum_{\mathbf{x}_S} \hat{V}_S(\mathbf{x}_B,\mathbf{x}_S,\omega)\hat{V}_0^*(\mathbf{x}'_A,\mathbf{x}_S,\omega) \approx$$
$$\int_{\partial D_{rec}} \rho c\hat{G}(\mathbf{x}_B,\mathbf{x}_A,\omega)\left[\sum_{\mathbf{x}_S}\hat{V}_0(\mathbf{x}_A,\mathbf{x}_S,\omega)\hat{V}_0^*(\mathbf{x}'_A,\mathbf{x}_S,\omega)\right]d^2\mathbf{x}_A \quad (2)$$

where $\mathbf{x}'_A$ as another receiver in the array. We discretize equation 2 in terms of monochromatic matrices $\hat{\mathbf{V}}_\mathbf{0}$, $\hat{\mathbf{V}}_\mathbf{S}$ and $\hat{\mathbf{G}}$, representing $\hat{V}_0$, $\hat{V}_S$ and $\hat{G}$, respectively, where the columns host (real or virtual) sources and the rows host receivers (Berkhout, 1982). The scaled impulse response can be retrieved with a stabilization parameter ε:

$$\rho c\hat{\mathbf{G}} \approx \hat{\mathbf{V}}_\mathbf{S}\hat{\mathbf{V}}_\mathbf{0}^\dagger\left[\hat{\mathbf{V}}_\mathbf{0}\hat{\mathbf{V}}_\mathbf{0}^\dagger + \varepsilon^2\mathbf{I}\right]^{-1}. \quad (3)$$

where the superscript $\dagger$ denotes the complex conjugate transpose. Implementation of equation 3 requires separation of incident and scattered wavefields for each individual subsurface source, which poses a major limitation. Assume that the incidence field cannot be separated from the total field $\hat{\mathbf{V}}$. However, we can still compute

$$\hat{\mathbf{V}}\hat{\mathbf{V}}^\dagger = \hat{\mathbf{V}}_\mathbf{0}\hat{\mathbf{V}}_\mathbf{0}^\dagger + \left[\hat{\mathbf{V}}_\mathbf{S}\hat{\mathbf{V}}_\mathbf{0}^\dagger + \hat{\mathbf{V}}_\mathbf{0}\hat{\mathbf{V}}_\mathbf{S}^\dagger\right] + \hat{\mathbf{V}}_\mathbf{S}\hat{\mathbf{V}}_\mathbf{S}^\dagger. \quad (4)$$

The first term in equation 4 will have its major contribution close $t = 0$. The term between the square brackets will have its dominant contributions at $|t| \geq t_1$, where t_1 is the two-way travel-time of the first reflector. If this reflector is located sufficiently deep, we can separate the first term in equation 4 from the term between the square brackets by time-gating after cross-correlation. The last term $\hat{\mathbf{V}}_\mathbf{S}\hat{\mathbf{V}}_\mathbf{S}^\dagger$ is relatively weak and we assume it can be neglected. Wapenaar and Fokkema (2006) show how an integral (or sum) over transient sources can be replaced by an ensemble average over simultaneously acting noise sources. We apply similar logic to equation 2 to show that

$$\left\langle \hat{V}_S(\mathbf{x}_B,\omega)\hat{V}_0^*(\mathbf{x}'_A,\omega)\right\rangle \approx$$
$$\int_{\partial D_{rec}} \rho c\hat{G}(\mathbf{x}_B,\mathbf{x}_A,\omega)\left\langle \hat{V}_0(\mathbf{x}_A,\omega)\hat{V}_0^*(\mathbf{x}'_A,\omega)\right\rangle d^2\mathbf{x}_A. \quad (5)$$

$\hat{V}_0(\mathbf{x}_A,\omega)$ (or $\hat{V}_0(\mathbf{x}'_A,\omega)$) and $\hat{V}_S(\mathbf{x}_B,\omega)$ are the incident field in $\mathbf{x}_A$ (or $\mathbf{x}'_A$) and the scattered field in $\mathbf{x}_B$ from simultaneously acting noise sources and $\langle\cdot\rangle$ is an ensemble average.

$\left\langle \hat{V}_S(\mathbf{x}_B,\omega)\hat{V}_0^*(\mathbf{x}'_A,\omega)\right\rangle$ and $\left\langle \hat{V}_0(\mathbf{x}_A,\omega)\hat{V}_0^*(\mathbf{x}'_A,\omega)\right\rangle$ can be estimated from $\left\langle \hat{V}(\mathbf{x}_A,\omega)\hat{V}^*(\mathbf{x}'_A,\omega)\right\rangle$ and $\left\langle \hat{V}(\mathbf{x}_B,\omega)\hat{V}^*(\mathbf{x}'_A,\omega)\right\rangle$ by time-gating after correlation. If we compute these crosscorrelations over sufficient receiver locations $\mathbf{x}_A$, equation 5 can be inverted, yielding an estimate of the scaled unknown Green's function $\rho c\hat{G}(\mathbf{x}_B,\mathbf{x}_A,\omega)$. This method can compensate for anisotropic illumination by simultaneously acting passive noise sources, as we will show with an example.

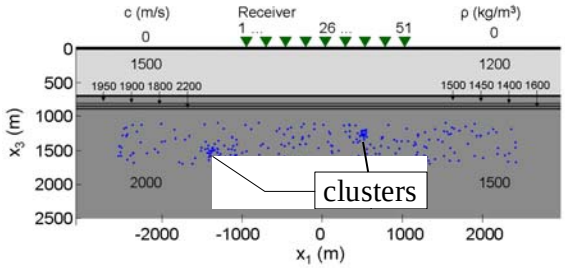

Figure 2: Configuration for the passive example; receivers are indicated by green triangles, sources by blue dots; we indicate the presence of two source clusters.

Example

The configuration for the passive example is shown in Figure 2. 51 vertical-component receivers are located at the earth's surface every 40 m. 200 passive sources are located in the subsurface with an irregular distribution with average spacing of 25 m; additionally, two source clusters are superimposed (with 20 and 30 sources, respectively). In Figures 3a-3c we show the individual components of the $\hat{\mathbf{V}}\hat{\mathbf{V}}^\dagger$-correlation at receiver 26. In Figure 4a we show their superposition. An estimation of the $\hat{\mathbf{V}}_\mathbf{0}\hat{\mathbf{V}}_\mathbf{0}^\dagger$- and $\hat{\mathbf{V}}_\mathbf{0}\hat{\mathbf{V}}_\mathbf{S}^\dagger$-response (Figures 3a and 3b) can be easily obtained from the $\hat{\mathbf{V}}\hat{\mathbf{V}}^\dagger$-gather (Figure 4a) by isolating all events $|t| < 0.5$s and $t > 0.5$s, respectively. The $\hat{\mathbf{V}}_\mathbf{S}\hat{\mathbf{V}}_\mathbf{S}^\dagger$-response (Figure 3c) is indeed weak and can be neglected. In Figure 4b we compare a slice of the retrieved reflection response by cross-correlation (followed by time-gating), with a reference response that is computed with an active source at the virtual source location. The retrieval is imperfect due to the presence of the source clusters. In Figure 4c we see the result after multi-dimensional deconvolution. Note that the imprint of the clusters has been compensated. Next we repeat the procedure, but with simultaneously acting noise sources. In Figure 5a we show a slice of the ensemble average $\left\langle \hat{V}(\mathbf{x}_A,\omega)\hat{V}^*(\mathbf{x}'_A,\omega)\right\rangle$. Compared to the transient

sources (Figure 4a), the cross-correlated wavelet signature seems slightly different and the record is noisier. However, the same spatial imprint of the source clusters can be observed. We can separate $\left\langle \hat{V}_0(\mathbf{x}_A,\omega)\hat{V}_0^*(\mathbf{x}'_A,\omega)\right\rangle$ and $\left\langle \hat{V}_S(\mathbf{x}_B,\omega)\hat{V}_0^*(\mathbf{x}'_A,\omega)\right\rangle$ (from $\left\langle \hat{V}(\mathbf{x}_B,\omega)\hat{V}^*(\mathbf{x}'_A,\omega)\right\rangle$) by isolating all events $|t|<0.5s$ and $t\geq 0.5s$, respectively. With this procedure we can retrieve the reflection response either through cross-correlation (Figure 5b) or multi-dimensional deconvolution (Figure 5c). Note that the latter has largely removed the imprint of the noise-source clusters at the cost of some inversion artifacts due to the noisy character of the data.

Conclusion

The reflection response as retrieved by cross-correlation of ambient-noise recordings is blurred by an imprint of the subsurface source distribution. This imprint (or point spread function) can be found in the retrieved response cluttered around t = 0 in the cross-correlation panels. We showed that if the first reflection is sufficiently deep, the imprint could be isolated by time-gating after cross-correlation and used for multi-dimensional deconvolution. We showed that this procedure can correct for anisotropic illumination of subsurface noise sources.

Acknowledgements

This work is supported by The Netherlands Research Centre for Integrated Solid Earth Science (ISES); the Netherlands Organisation for Scientific Research (NWO, Toptalent 2006 AB); and the Dutch Technology Foundation (STW), an applied science division of NWO and the technology program of the Ministry of Economic Affairs (grant DCB.7913).

References

Berkhout A.J., 1982. Seismic migration. Imaging of acoustic energy by wave field extrapolation. *Elsevier*.

Draganov D., Campman X., Thorbecke J., Verdel A. and Wapenaar K., 2009, Reflection images from ambient seismic noise. *Geophysics*, **74**, A63-A67.

Menke W., 1989. Geophysical data analysis. *Academic Press*, San Diego, CA.

Van Groenestijn G.J.A. and Verschuur D.J., 2009, Estimation of primaries by sparse inversion from passive seismic data. 79th International Meeting Society of Exploration Geophysicists, expanded abstracts, 1597-1601.

Wapenaar K. and Fokkema J., 2006. Green's function representations for seismic interferometry. *Geophysics*, **71**, SI33-SI46.

Wapenaar K., Van der Neut J. and Ruigrok E., 2008. Passive seismic interferometry by multidimensional deconvolution. *Geophysics*, **73**, A51-A56.

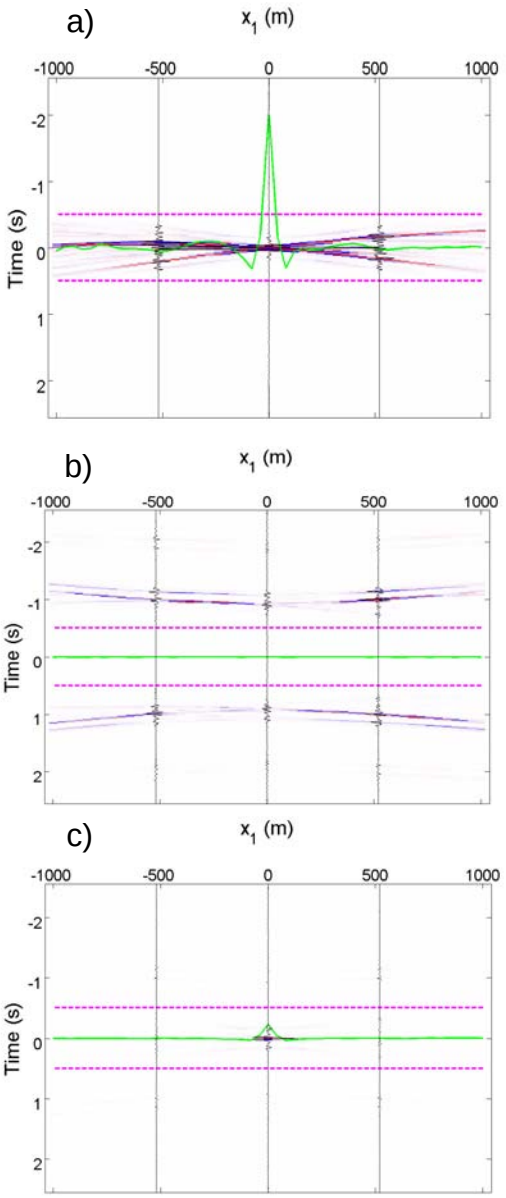

Figure 3: (a) Slice of $\hat{\mathbf{V}}_0\hat{\mathbf{V}}_0^{\dagger}$, (b) slice of $\hat{\mathbf{V}}_S\hat{\mathbf{V}}_0^{\dagger}+\hat{\mathbf{V}}_0\hat{\mathbf{V}}_S^{\dagger}$, (c) slice of $\hat{\mathbf{V}}_S\hat{\mathbf{V}}_S^{\dagger}$; all gathers have a similar amplitude scale and a virtual source at receiver 26; the maximum in (a) is clipped; in green we show a spatial trace at t=0, in black we show three temporal traces and in pink we show the time-gate.

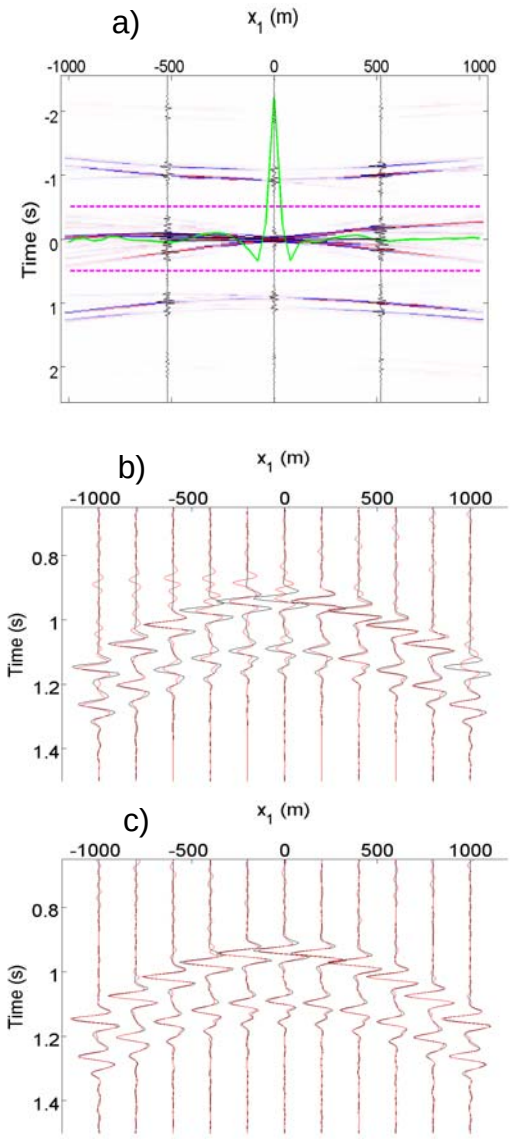

Figure 4: (a) Slice of $\hat{\mathbf{V}}\hat{\mathbf{V}}^{\dagger}$ at virtual source 26; retrieved response by (b) cross-correlation and (c) multi-dimensional deconvolution (both in red) versus the reference response (in black) using time-gating after cross-correlation from transient sources and a virtual source at receiver 26.

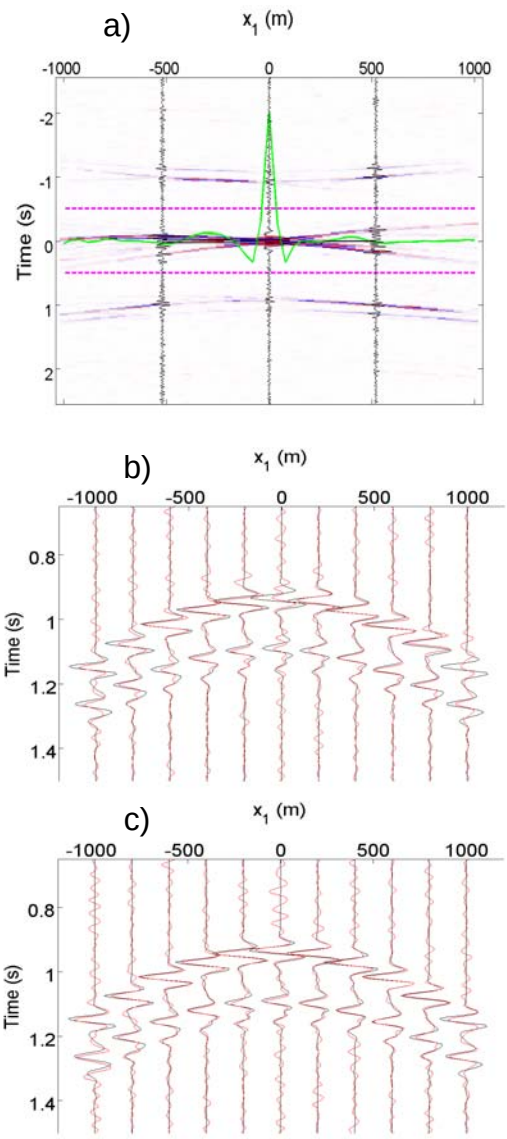

Figure 5: (a) Slice of $\left\langle \hat{V}\left(\mathbf{x}_A,\omega\right)\hat{V}^{*}\left(\mathbf{x}'_A,\omega\right)\right\rangle$ at virtual source 26; retrieved response by (b) cross-correlation and (c) multi-dimensional deconvolution (both in red) versus the reference response (in black) using time-gating after cross-correlation from simultaneously acting noise sources and a virtual source at receiver 26.